Atmospheric aerosol properties over the equatorial Indian Ocean and the impact of the Madden-Julian Oscillation

H. Langley DeWitt,[1,2] Derek J. Coffman,[1] Kristen J. Schulz,[1] W. Alan Brewer,[3] Timothy S. Bates,[1] and Patricia K. Quinn[1]

Received 15 October 2012; revised 15 April 2013; accepted 16 April 2013; published 3 June 2013.

[1] The chemical, physical, and optical properties of sub- and supermicrometer aerosols over the equatorial Indian Ocean were measured on board the R/V *Revelle* during the fall 2011 Dynamics of the Madden-Julian Oscillation field campaign. During this time, both the retreating of the Asian monsoon and two Madden-Julian Oscillation (MJO) events were observed. The R/V *Revelle* was on station (0.1°N and 80.5°E) to measure atmospheric and oceanic conditions between 4 October and 30 October 2011 (Leg 2) and 11 November and 4 December 2011 (Leg 3). Throughout the campaign, background marine atmospheric conditions were usually observed. As the Asian monsoon season retreated over the boreal fall and the general wind direction changed from southerly to northerly transporting, respectively, clean marine and polluted continental air masses, the average submicrometer aerosol mass nearly doubled from Leg 2 to Leg 3 and the aerosol appeared to be more influenced by continental sources. The effect of MJO-associated convection anomalies on aerosols in the remote marine boundary layer (MBL) was measured during November when a complete MJO convection wave moved over the equatorial Indian Ocean and during October when a partial MJO event was observed. MJO-associated convection strongly affected the local aerosol as increased vertical mixing introduced new particles into the MBL, rainout cleared the atmosphere of submicrometer aerosol particles, and high winds enhanced the concentration of sea salt aerosol particles in the local atmosphere. Four stages of MJO-affected aerosol population changes in the remote Indian Ocean are defined.

Citation: Langley DeWitt, H., D. J. Coffman, K. J. Schulz, W. Alan Brewer, T. S. Bates, and P. K. Quinn (2013), Atmospheric aerosol properties over the equatorial Indian Ocean and the impact of the Madden-Julian Oscillation, *J. Geophys. Res. Atmos.*, *118*, 5736–5749, doi:10.1002/jgrd.50419.

1. Introduction

[2] The Madden-Julian Oscillation (MJO) [*Lau and Waliser*, 2012; *Madden and Julian*, 1972; *Zhang*, 2005] is one of the largest source of sub-seasonal weather variability in the tropics and has been linked to large-scale weather and climate phenomena such as the El Nino Southern Oscillation [*Kessler and McPhaden*, 1995], variability in the strength of the monsoon season in Asia and Africa [*Annamalai and Slingo*, 2001], and the formation and propagation of tropical cyclones [*Liebmann et al.*, 2004]. Predictability of the initiation and propagation of the MJO in the equatorial Indian Ocean, and thus its effects on local and global scale weather patterns, is currently quite low. To increase scientific understanding of the oceanic and atmospheric processes governing the MJO initiation, the Dynamics of the Madden-Julian Oscillation (DYNAMO) field campaign took place in conjunction with the international Cooperative Indian Ocean Experiment on Intraseasonal Variability in the equatorial Indian Ocean during the boreal fall and winter of 2011/2012 [*Yoneyama et al.*, 2013]. Two ground sites (Gan and Diego Garcia) and two shipboard sites (the R/V *Revelle* and the R/V *Mirai*) were active during an intense measurement period from late September to mid-December. In addition, measurements were made at buoys and atmospheric sounding sites throughout the boreal fall and winter of 2011/2012. The R/V *Revelle* was stationed at approximately 0.1°N and 80.5°E and carried on board a suite of instruments designed to characterize the composition of the atmosphere and ocean from 200 m above to 200 m below the ocean's surface. A subset of these measurements was focused on the characterization of the physical, chemical, and optical properties of aerosols in the remote equatorial Indian Ocean.

[1]Pacific Marine Environmental Laboratory, NOAA, Seattle, Washington, USA.
[2]Aix Marseille Univ., Laboratoire Chemie Environnement (LCE), Equipe Instrumentation et Réactivité Atmosphérique (IRAA), Marseille, France.
[3]Earth System Research Laboratory, NOAA, Boulder, Colorado, USA.

Corresponding author: H. Langley DeWitt, Aix Marseille Univ., Laboratoire Chemie Environnement (LCE), Equipe Instrumentation et Réactivité Atmosphérique (IRAA), 13 331 Marseille, France. (langleydew@gmail.com; helen-langley.dewitt@univ-amu.fr)

2169-897X/13/10.1002/jgrd.50419

[3] Aerosols can perturb the earth's radiation balance directly through the scattering (e.g., by sea salt) and absorption (e.g., by soot) of incoming solar radiation and indirectly through aerosol-cloud interactions that can change the microphysical properties, lifetime, and extent of clouds. The sources of aerosol in a given region affect the chemical, physical, and optical properties of the aerosol, the total aerosol concentration, and its climate forcing capability and influence on local weather patterns. In the equatorial Indian Ocean, southerly winds bring background marine air and northerly winds bring continental air from Asia. The typically low biological primary productivity in the Indian Ocean [*Dasgupta et al*., 2009] and low-wind speeds over the equator reduce the influence of biogenic emissions and primary marine emissions on aerosol properties. During the fall season, the wind direction over the Indian Ocean changes from primarily southerly to primarily northerly as the Asian summer monsoon retreats. Large differences in the properties of aerosol from the northern hemisphere (NH) versus the southern hemisphere (SH) have been observed, with higher submicrometer mass concentration and absorption observed in NH aerosol [*Quinn et al*., 2002; *Ramanathan et al*., 2001; *Spencer et al*., 2008].

[4] An MJO event is characterized by a period of enhanced convection preceded and followed by periods of suppressed convection. Anomalous low level easterly (preceding) and westerly (following) winds flank the enhanced convection of the MJO, combined with an overturning of the troposphere [*Zhang*, 2005]. These changing wind directions introduce new aerosol mass to the equatorial ocean, and air masses from the upper atmosphere are mixed down into the MBL as the troposphere overturns. Increased wind speeds, often in the form of a westerly wind burst, are common during and following the enhanced MJO convection [*Zhang*, 2005]. High winds are associated with increases in primary marine aerosol, thus the enhanced convection from an MJO event may introduce more sea spray aerosol mass to the atmosphere. The suppressed convection periods, with low-wind speeds and dry conditions, could affect aerosol concentration in the opposite way such that primary marine aerosol would be reduced due to low winds and calm ocean conditions. However, secondary marine and transported continental aerosol could build up in the atmosphere during the suppressed phase due to dry conditions and subsequently reduced rainout rates. The MJO is more active during boreal winter when the Australian monsoon is active [*Zhang*, 2005]. During this time, continental aerosol concentrations are also greatest over the equatorial ocean. As the MJO could affect the aerosol population in the MBL, the aerosol's direct and indirect effects on the local cloud and radiative budget could also affect the MJO convection.

[5] Previous work has analyzed aerosol, carbon dioxide, and ozone (O_3) data from satellite observations to determine the effect of enhanced convection (as indicated by rainfall) associated with an MJO event on aerosol and gas concentrations [*Li et al*., 2010; *Tian and Waliser*, 2012; *Tian et al*., 2007; *Tian et al*., 2008]. Convection associated with the MJO (i.e., vertical motions in the atmosphere, rainfall) was found to affect the concentrations of these species in the remote marine atmosphere [*Li et al*., 2010; *Tian et al*., 2007, 2008]. The Aerosol Index (AI) calculated from the Total Ozone Mapping Spectrometer (TOMS), which measures the concentration of ultraviolet absorbing aerosols (e.g., smoke, dust, and ash), was found to have negative anomalies at times when the rainfall in the area was found to have positive anomalies. In other words, increased rainfall led to decreased absorbing aerosol in the atmosphere, likely through wet deposition, although possibly due to a sampling artifact in the TOMS AI data [*Tian et al*., 2008]. Moderate Resolution Imaging Spectroradiometer (MODIS) data were used to study the relation of MJO phase and fire count in the maritime continent of Malaysia and Indonesia where biomass burning provides a large source of submicrometer aerosol [*Reid et al*., 2012]. The authors found that while the active phase of the MJO was over the Indian Ocean fires were suppressed, which would also decrease the concentration of absorbing aerosols in the Indian Ocean [*Reid et al*., 2012]. In contrast, the Aerosol Optical Thickness (AOT) derived from the MODIS, which measures both absorbing and non-absorbing aerosols, was found to have a positive anomaly weakly correlated to positive rainfall anomalies [*Tian et al*., 2008]. An increase in sea salt aerosol concentrations due to increased wind speeds concurrent with the enhanced MJO rainfall may be one cause of this observation [*Tian et al*., 2008]. Cloud contamination in the satellite signal and an imperfect cloud retrieval algorithm is also discussed as another reason for this correlation between rainfall and increased AOT [*Tian et al*., 2008]. In situ measurements of the aerosol response to MJO convection are essential to increase scientific understanding of the feedback between the MJO and aerosol.

[6] Here, we discuss the in situ aerosol measurements made on board the R/V *Revelle* throughout the shoulder season (September through October) and beginning of the dry season (November onwards) of the Asian monsoon over the equatorial Indian Ocean. This data set represents the first in situ measurements of the effect of MJO-related convection on aerosol properties in the remote Indian Ocean. We specifically focus on the changing aerosol population as the Asian monsoon retreats and on the aerosol response to a fully observed MJO event in late November. By examining the effect of intraseasonal (MJO events) and seasonal (the Asian monsoon) convection on aerosols, we hope to understand the feedback between routinely occurring climatological events and aerosol concentration in the remote Indian Ocean. The implications of these observations are discussed.

2. Measurements

[7] Aerosol measurements onboard the R/V *Revelle* during DYNAMO included real-time (5 min. time resolution) and filter-based (12 to 24 h time resolution) analyses of aerosol chemical composition, size, concentration, and optical properties. Aerosol measurements were made at 60% relative humidity (RH).

2.1. Aerosol Inlet

[8] An aerosol inlet 18 m above the surface of the ocean on the forward deck of the R/V *Revelle* was used to sample sub- (<1.1 μm in aerodynamic diameter at 60% RH) and supermicrometer (>1.1 μm in aerodynamic diameter at 60% RH) aerosol particles for both filter-based and real-time analysis. This inlet has been described in greater detail elsewhere [*Bates et al*., 2005, 2008; *Quinn et al*., 2008].

Briefly, flow was maintained at 1 $m^3 min^{-1}$, and the mast was heated at the bottom 1.5 m to maintain the RH of aerosols at $60 \pm 5\%$. The inlet has greater than 95% transmission efficiency for particles less than 6.5 μm based on wind tunnel tests [*Bates et al*., 2002]. To prevent contamination from the ship's stack, an anemometer and computer control were used to automatically shut off flow through the impactors in the case of wind from the aft of the ship (relative wind direction of $\pm 100°$ off the bow) or wind speed below 0.5 $m s^{-1}$. In addition, the mast was automated to turn into the wind to maintain pseudo iso-kinetic flow to minimize particle losses. Particle number concentrations and relative wind direction were used to remove sampling periods from the real-time data that appeared to be contaminated by the ship's exhaust.

2.2. Impactor Measurements

[9] Two and seven stage multi-jet cascade impactors [*Berner et al*., 1979] with sampling times of 12–24 h were used to determine sub- and supermicrometer concentrations of aerosol mass, inorganic ions (chloride (Cl^-), nitrate (NO_3^-), sulfate (SO_4^{-2}), methanesulfonate (MSA^-), bromide (Br^-), oxalate ($C_2O_4^{-2}$), sodium (Na^+), ammonium (NH_4^+), potassium (K^+), magnesium (Mg^{+2}), calcium (Ca^{+2})), and total carbon (TC). Specific details on the impactor methods and filters used are described in *Bates et al*. [2005]. Inorganic ion concentrations were measured using ion chromatography (IC) [*Quinn and Coffman*, 1998]. TC concentration was measured using a Sunset Laboratories OC/EC thermal/optical analyzer instrument. Elemental carbon (EC) was close to blank levels for the samples collected, thus organic carbon (OC) and EC are reported together here as TC. The thermal program was the same as that used in previous field campaigns [*Bates et al*., 2012].

[10] A two-stage multi-jet cascade impactor sampling at 60% RH was used to determine the sub-1.1 μm and 1.1–10 μm diameter aerosol mass. Millipore Fluoropore films and Teflo filters were used in the impactor. Films were cleaned in an ultrasonic bath in 10% H_2O_2 for 30 min, rinsed in distilled, deionized water, and dried in an NH_3^- and SO_2-free glove box. Films and filters were weighed back in the laboratory with a Cahn Model 29 and Sartorius model SE2 balance, respectively. The balances are housed in a glove box kept at a humidity of $65 \pm 4\%$. The resulting mass concentrations from the gravimetric analysis include the water mass that is associated with the aerosol at 65% RH.

[11] The glove box was continually purged with room air that had passed through a scrubber of activated charcoal, potassium carbonate, and citric acid to remove gas phase organics, acids, and ammonia. Static charging, which can result in balance instabilities, was minimized by coating the walls of the glove box with a static dissipative polymer (Tech Spray, Inc.), placing an anti-static mat on the glove box floor, using anti-static gloves while handling the substrates, and exposing the substrates to a 210Po source to dissipate any charge that had built up on the substrates. Before and after sample collection, substrates were stored double-bagged with the outer bag containing citric acid to prevent absorption of gas phase ammonia. More details of the weighing procedure can be found in previous papers [*Quinn and Coffman*, 1998].

2.3. Aerosol Mass Spectrometry

[12] An Aerodyne Quadrupole Aerosol Mass Spectrometer (Q-AMS) was used to measure the chemical composition of submicrometer non-refractory aerosol particles [*Canagaratna et al*., 2007] in real-time. Sample air was drawn from the inlet (section 2.1), through an impactor with a jet plate having a 50% aerodynamic cut-off diameter of 1.1 μm, through temperature controlled (23°C) stainless steel tubing and then into the Aerodyne aerodynamic lens. The aerodynamic lens has an approximate 100% transmission efficiency for particles 70–500 nm in diameter. For particles with vacuum aerodynamic diameters between 30 to 70 nm and 500 nm to 1.0 μm, transmission efficiencies decrease from 100% to 50% [*Bates et al*., 2008; *Canagaratna et al*., 2007]. Gaseous species are pumped away upon entering the instrument measurement chamber. A rotating chopper is used to set start times for aerodynamic sizing from particle flight time in the time of flight (ToF) chamber and to block aerosol flow to measure the instrument background. Particles exiting the ToF chamber are vaporized at approximately 600°C, ionized at 70 eV using electron ionization, and analyzed using a quadrupole mass spectrometer. Measured species include organics, SO_4^{-2}, NO_3^-, and NH_4^+. Five-minute averages of the aerosol mass spectrum (in terms of mass-to-charge ratios m/z) were collected. Limits of detection were calculated using the method described by *Bates et al*. [2008] and *DeCarlo et al*. [2006] and were found to be 0.31 μg m^{-3} for organics, 0.25 μg m^{-3} for NH_4^+, 0.02 μg m^{-3} for NO_3^-, and 0.04 μg m^{-3} for SO_4^{-2}. The collection efficiency was calculated to be 1.0 for data collected from 1 October to 29 November and 0.75 for data collected from 29 November onward. The collection efficiency was calculated by comparing concentrations of SO_4^{-2} measured by the AMS to those derived from the impactor/IC measurements.

2.4. Aerosol Size and Optical Property Measurements

[13] Aerosol size distributions from 0.02 to 10 μm geometric diameter were measured using three different instruments at 60% RH including an ultrafine differential mobility particle sizer (from 3 to 26 nm), a differential mobility particle sizer (from 20 to 671 nm), and an aerodynamic particle sizer (APS, from 0.542 to 20 μm). APS diameters were originally measured in aerodynamic diameters and converted to geometric diameters. Exact specifications are described by *Bates et al*. [2005]. Distributions were sampled every 15 min.

[14] Sub-10 (aerosols with geometric diameters <10 μm) and submicrometer aerosol scattering coefficients were measured at 60% RH with two integrating nephelometers (Model 3563, TSI, Inc.) at three wavelengths (450, 550, and 700 nm). Scattering coefficients were corrected for any offset using filtered air and also for instrument error and non-ideality [*Anderson and Ogren*, 1998]. The sub-10 micrometer aerosol scattering coefficient measurement error varied from ± 3.8 Mm^{-1} for the maximum measured scattering coefficient of 450 Mm^{-1} to 0.7 Mm^{-1} for the minimum measured scattering coefficient of 12 Mm^{-1}.

[15] A separate humidity controlled system measured submicrometer light scattering at low and high humidity with two TSI integrating three-wavelength nephelometers operated in series downstream of a Berner impactor. The

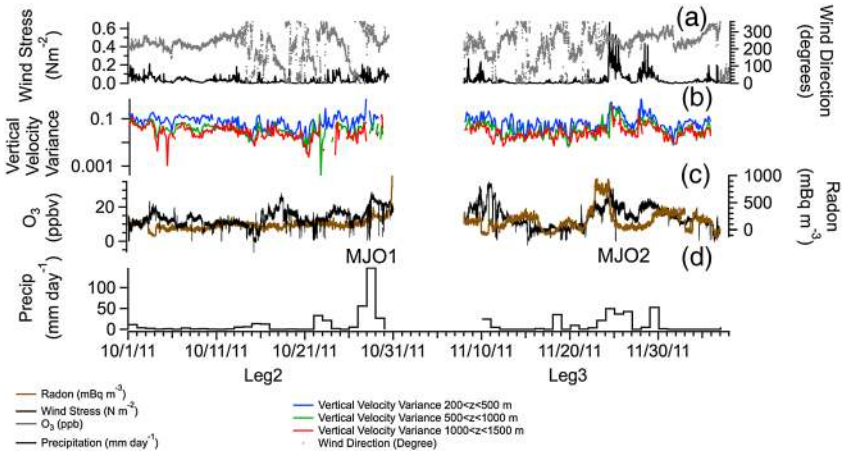

Figure 1. (a) Wind stress (Nm^{-2}) (left axis), Wind direction (right axis in Figure 1a), (b) Vertical Velocity Variance, (c) Ozone (O_3) (left axis), Radon, $mBqm^{-3}$ (right axis in Figure 1c), and (d) Precipitation ($mm\,day^{-1}$).

60% RH conditioned aerosol from the inlet was dried to 25% RH using a PermaPure, multiple-tube Nafion dryer model PR-94. The first nephelometer measured scattering of the 25% RH aerosol. Downstream of this nephelometer, a humidifier was used to add water vapor to the sample flow (six microporous Teflon tubes surrounded by a heatable water-jacket). The sample was conditioned to approximately 85% RH, and the scattering of these humidified particles was measured by the second TSI nephelometer. Humidity was measured with a chilled mirror dew point hygrometer downstream of the second nephelometer. The slope of a regression between the high and low RH scattering coefficients was used to scale scattering measurements made at 60% RH to aerosol scattering at ambient RH.

[16] Sub-10- and submicrometer aerosol absorption coefficients were measured using two particle soot absorption photometers at three wavelengths (467, 530, and 660 nm). Error varied from $\pm 0.4\,Mm^{-1}$ for an absorption measurement of $4.6\,Mm^{-1}$ to ± 0.08 for absorption measurements $<0.1\,Mm^{-1}$.

[17] A handheld Microtops sunphotometer (Solar Light Co.) with five channels (380, 440, 500, 675, and 870 nm) was used to derive AOT. The raw Microtops data were processed and used to calculate AOT by the NASA Maritime Aerosol Network in conjunction with the Aerosol Robotic Network [*Smirnov et al.*, 2009]. Data were only collected during days when there were no visible clouds in the path between the ship location and the sun.

2.5. Additional Measurements

[18] Radon (an indicator of air masses recently over land) and ozone (O_3), an indicator of air masses mixed down from the upper atmosphere, were also measured on the ship. Air was sampled from 18 m above sea level down the 20 cm inner diameter (ID) powder coated aluminum aerosol sampling mast (6 m) at approximately $1\,m^3\,min^{-1}$. At the base of the sampling mast, a $1\,L\,min^{-1}$ flow was pulled through a 0.32 cm ID, 2 m long Teflon tube into a Thermo Environmental Instruments Model 49c ozone analyzer. The data have been filtered to remove zero-air periods and periods of obvious ship contamination from the R/V *Revelle*. Radon gas was measured using a dual flow loop, two-filter radon detector [*Whittlestone and Zahorowski*, 1998]. The sample flow rate into and out of the tank was typically $70\,L\,min^{-1}$. The response time of the radon instrument is limited to about 30 min by the radiological decay time constants of the radon daughters on the wire screen filter. The instrument was calibrated with a known radon source in Seattle on 7 June 2011.

[19] NOAA's High Resolution Doppler Lidar (HRDL) provided profiles of the horizontal wind speed, aerosol backscatter intensity, and vertical velocity variance within the MBL every 20 min throughout Legs 1–3 of the campaign. HRDL utilizes a motion-stabilized hemispheric scanner to orient the beam in the atmosphere, and a high-repetition-rate, solid state laser operating at a 2.02 μm wavelength provides 30 m range resolved measurements of the line-of-sight wind speed and aerosol backscatter intensity twice a second [*Grund et al.*, 2001; *Tucker et al.*, 2009]. Aerosol backscatter intensity measurements were most sensitive to supermicrometer aerosols due to the wavelength of the laser [*Grund et al.*, 2001]

[20] Meteorological data (wind speed, stress and direction, temperature, and precipitation rate) and oceanographic (significant wave height) were also collected. Seven-day back trajectories from the Hybrid Single Particle Lagrangian Integrated Trajectory Model (HYSPLIT, NOAA) were run for three arrival heights—200, 1000, and 3000 m—at 24 h increments to determine the approximate source, transport path, and age of aerosols measured at the ship site.

3. Experimental Conditions

3.1. Convection Over the DYNAMO Experiment as Measured Onboard the R/V Revelle

[21] We show the changing vertical velocity variance (column averaged over three altitude ranges), precipitation, O_3, radon, wind direction, and wind stress in Figure 1 for the entire October–December sampling period. Noted are the two Madden-Julian Oscillation events, MJO1 (enhanced convection beginning on 30 October) and MJO2 (enhanced convection beginning on 24 November) [*Yoneyama et al.*, 2013]. Detailed descriptions of MJO-related convection as observed during DYNAMO are beyond the scope of our measurements and will be analyzed

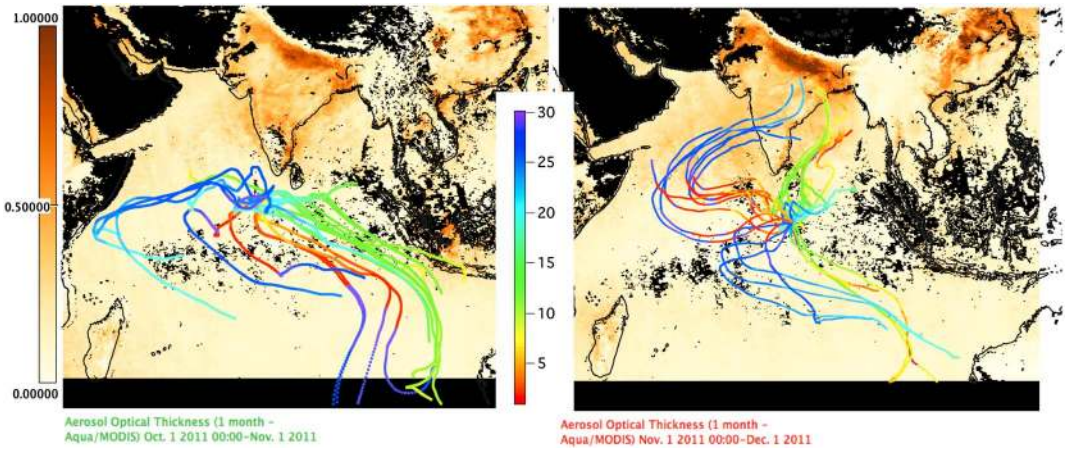

Figure 2. HYSPLIT 7 day calculated air mass backtrajectories at an arrival height at the ship of 200 m for Leg 2 (Figure 2, left; 4 October–30 October) and Leg 3 (Figure 2, right; 11 November–4 December). Day of the month indicated by color (see rainbow color scale). Trajectories are overlaid on the average aerosol optical thickness from MODIS Aqua Satellite data for October (Figure 2, left) and November (Figure 2, right).

by other research groups and reported in the future. The MJO index [*Wheeler and Hendon*, 2004] reported by *Yoneyama et al.* [2013] for the entirety of DYNAMO observations shows that clear anomalies of outgoing longwave radiation and zonal winds characteristic of MJO-related convection were observed over the Indian Ocean during the month of November.

[22] At the ship location, rainfall and high wind stress observed shipboard on 24 November flanked on either side by periods of low wind and dry conditions, indicate that the full MJO cycle was observed by instruments onboard the R/V *Revelle*. Increases in precipitation for MJO1 and MJO2 are clearly visible in Figure 1. While the wind stress increased for MJO1, the magnitude of the wind stress increase was less for MJO1 than for MJO2. The vertical velocity variance, a good indicator of local mixing and vertical transport, also increased during the periods before and during MJO enhanced convection. The combination of increased vertical velocity variance along with increased O_3 indicates that there was more downward motion in the lower atmosphere just prior to and during the MJO convection.

3.2. Changing Aerosol Transport Direction as the Asian Summer Monsoon Retreats

[23] MODIS-derived AOT from the Aqua satellite for the months of October and November (2011) is shown for the Indian Ocean in Figure 2. The dark areas south of the equator are due to cloud coverage related to the intertropical convergence zone [*Yoneyama et al.*, 2013]. For both October and November, AOT values ranged from around 0.16 (mid-ocean) to 0.5 (Indian subcontinent). However, the direction of the calculated air mass back trajectories, also shown in Figure 2, reversed from primarily southerly to primarily northerly as the boreal fall progressed and the Asian monsoon retreated. The change from southerly to northerly flow resulted in an increase in the transport of continental and anthropogenic aerosol from India and Sri Lanka to the equatorial Indian Ocean.

4. Aerosols Over the Indian Ocean

4.1. Aerosol Properties During Monsoon Reversal

[24] Due to the change in wind direction over the Indian Ocean from southerly to northerly that accompanied the onset of the dry season, continental aerosol was observed more frequently in the later months of the DYNAMO research project. Figure 3 shows the time series concentration of SO_4^{-2}, organics, and NH_4^+ for both Leg 2 and Leg 3. Also shown are impactor measurements of MSA^-, K^+, and radon as well as the gravimetric mass concentration of supermicrometer aerosol. As the Asian monsoon retreated over October and November, note the increase in periods of enhanced radon and enhanced submicrometer particles (Figure 3). The average submicrometer aerosol mass concentration almost doubled from Leg 2 to Leg 3 (increasing from $1.8 \pm 1.1\ \mu g\ m^{-3}$ to $3.3 \pm 2.2\ \mu g\ m^{-3}$). For both legs, the submicrometer aerosol was primarily SO_4^{-2} in composition. On average, the molar ratio of NH_4^+ to SO_4^{-2} was around one throughout the field campaign (0.98 ± 0.18 for Leg 2, 0.93 ± 0.14 for Leg 3). As the submicrometer aerosol concentration increased, the AOT (500 nm) measured aboard the ship nearly doubled from Leg 2 to Leg 3 (0.07 ± 0.02 to 0.13 ± 0.05). Note that the average supermicrometer aerosol mass remained approximately the same, increasing slightly from an on-station average of 7.8 ± 4.5 (Leg 2) to $9.3 \pm 8.4\ \mu g\ m^{-3}$ (Leg 3), and was primarily sea salt in composition. The largest concentrations of supermicrometer aerosol were observed during enhanced convection associated with MJO1 and MJO2. The overall rise in submicrometer aerosol mass and AOT over the measurement period is likely due to the increase in anthropogenic aerosol over the Indian Ocean in the boreal winter.

4.2. Investigation of Specific Aerosol Sources to the MBL: Marine and Continental

[25] Aerosol particles can be introduced to the remote MBL through a variety of sources [*Quinn and Bates*, 2011], including long-range transport from continental regions, primary ocean-derived sea spray aerosol formed

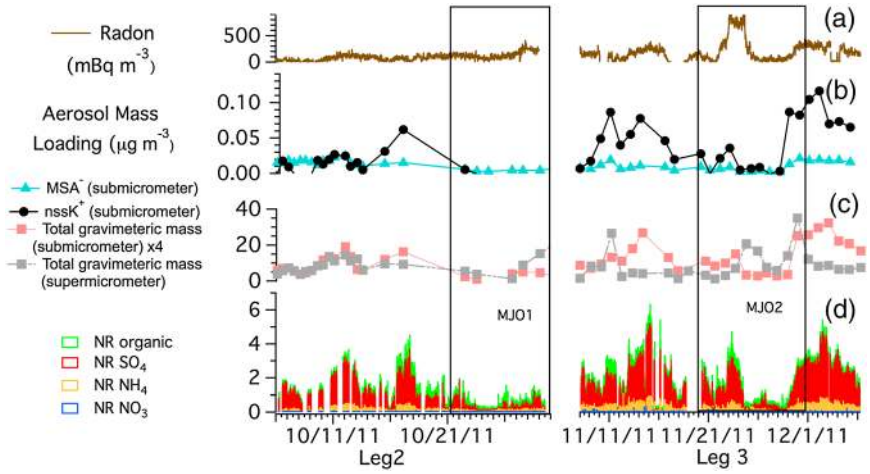

Figure 3. (a) Radon, (b) impactor measurements of submicrometer non-sea salt potassium (K^+) and methylsulfonic acid (MSA^-) (b), (c) gravimetric submicrometer and supermicrometer aerosol mass concentration, (d) and non-refractory (NR) submicrometer concentrations of sulfate (SO_4^{-2}), organic, ammonia (NH_4^+), and nitrate (NO_3^-) aerosol from Quadrupole Aerosol Mass Spectrometry measurements.

through wind-driven bubble bursting at the ocean surface [*de Leeuw et al*., 2011; *O'Dowd et al*., 2008], and the mixing down of particles formed in the free troposphere [*Clarke et al*., 1998b]. Once in the remote MBL, aerosol particles become further processed by gas to particle conversion, heterogeneous reactions, photochemical aging, and cloud processing. The result is a mixture of aerosol particles from different sources modified both chemically and physically since emission. Wind speed and direction, vertical mixing, and precipitation all affect aerosol formation, lifetime, and transport in the remote marine environment. Here we discuss the specific types and sources of aerosol observed during October, November, and December 2011 on the equatorial Indian Ocean and show example mass spectra of each aerosol type.

[26] Although SO_4^{-2} dominated the submicrometer aerosol mass throughout the observation period, distinct aerosol events stood out from the marine background aerosol signal (defined by a threshold of approximately 1 μg m^{-3} of submicrometer aerosol mass (Figure 3)). The Q-AMS mass spectra, normalized to the highest mass peak, of four unique types of aerosol are shown in Figure 4. Sources of MBL aerosol during DYNAMO were investigated by assessing concentrations of inorganic ions, Q-AMS mass spectra, O_3, and radon (Figure 3). Specific aerosol types observed were: Primary marine aerosol measured during a period of high winds on 24 November (Figure 4a); a period of continental aerosol associated with easterly flow and a slight rise in radon on 17 October (Figure 4b); aerosol that was mixed down from the upper atmosphere to the MBL (here on 15 October), indicated by a period of enhanced O_3 and high vertical velocity variance as measured by the HRDL (Figure 4c); and aerosol measured during enhanced secondary marine particle production, indicated by an elevated peak in MSA concentration (here on 11 October) (Figure 4d). Each of these aerosol types had significant concentrations of SO_4^{-2} (1.5–4 μg m^{-3}) and organic aerosol (0.4–1μg m^{-3}).

[27] For both the high MSA period (11 October) and the continental period (17 October), the COO^+ peak (*m*/*z* 44), an indicator of aged/oxidized organic aerosol [*Zhang et al*., 2005a], contributed the most mass to the organic fraction of the aerosol. During the high MSA^- period on 11 October, hydrocarbon-like aerosol fragments also were observed, possibly from primary sea spray emissions [*Ovadnevaite et al*., 2011]. Additionally, *m*/*z* 79, which has been associated with a fragment of MSA^- ($CH_3SO_2^-$) in aerosol measured over the ocean [*Zorn et al*., 2008], was observed in the average mass spectrum during this time period.

[28] During the continental aerosol period (17 October), the 39/41 *m*/*z* peaks were significantly higher than during the other aerosol events. These peaks are most likely K^+ as the ratio of these two peaks in the averaged mass spectra is very close to the K39/K41 isotopic ratio. In the 15 October

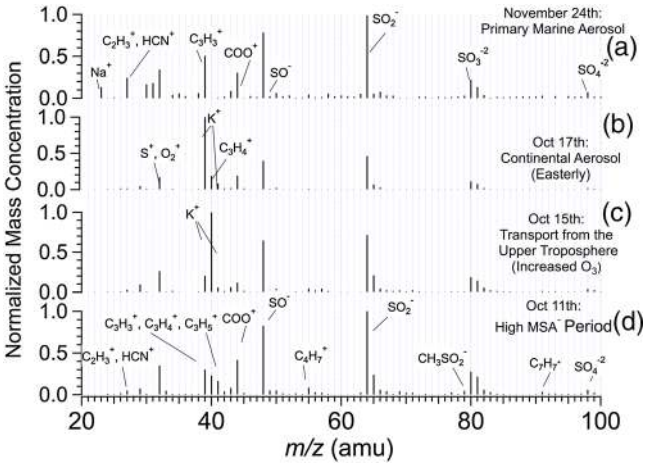

Figure 4. Normalized Quardupole Aerosol Mass Spectrometer spectra of four distinct aerosol events during (a) primary marine aerosol from a high wind event, (b) continental aerosol from easterly flow, (c) downward transport of aerosol to the marine boundary layer, and (d) aerosol from a high methyl sulfonic acid (MSA^-) period. The spectra have been normalized to the highest peak in the 20–100 *m*/*z* range to show each spectrum on the same scale. Filtered blank air has been subtracted from the mass spectra, as has the gas signal.

Table 1. Submicrometer Aerosol Inorganic and Organic Components (24 h Time Resolution) and Aerosol Single Scattering Albedo (SSA) Divided Into Sectors Based on Back Trajectory Analysis[a]

($\mu g\,m^{-3}$)	N	S	E	W	NHIO[b]	SHIO[b]
Sea Salt	0.05 ± 0.05	$.06 \pm 0.05$	0.03 ± 0.01	0.06 ± 0.01	0.09 ± 0.03	0.07 ± 0.08
NH_4	0.35 ± 0.23	0.12 ± 0.09	0.01 ± 0.01	0.20 ± 0.09	0.5 ± 0.12	0.09 ± 0.04
nssK	0.06 ± 0.04	0.03 ± 0.02	BDL	0.03 ± 0.02		
MSA	0.01 ± 0.006	0.01 ± 0.006	0.004 ± 0.001	0.02 ± 0.005		
NO_3	0.004 ± 0.004	0.009 ± 0.003	0.008 ± 0.003	0.01 ± 0.002	0.007 ± 0.007	<0.001
$nssSO_4$	1.95 ± 1.17	0.62 ± 0.42	0.09 ± 0.09	1.10 ± 0.53	1.8 ± 0.24	0.52 ± 0.18
Oxalate	0.006 ± 0.004	0.004 ± 0.004	0.001 ± 0.001	0.005 ± 0.004		
Total Carbon	0.45 ± 0.27	0.41 ± 0.31	0.18 ± 0.04	0.45 ± 0.14		
SSA[c]	0.96 ± 0.02	0.99 ± 0.01	0.98 ± 0.02	0.98 ± 0.01	0.91 ± 0.01	1.0 ± 0.02

[a]Data from the northern and southern hemisphere Indian Ocean [*Quinn et al*., 2002] are shown for comparison.
[b][*Quinn et al*., 2002].
[c]SSA calculated at 530 nm, sub-10-μm. DYNAMO data are calculated from 60% RH optical data corrected for ambient RH using f(RH)measurements. Sub-1-μm SSA for the INDOEX data was calculated at 75% RH [*Quinn et al*., 2002].

spectrum, the aerosols mixed down from the free troposphere were primarily composed of acidic sulfate. This finding agrees with previously reported results from both measurement and modeling studies [*Clarke et al*., 1998b] of the nucleation of new particles from water vapor and H_2SO_4 in the free troposphere. Both anthropogenic sources and marine sources (such as the photooxidation of dimethyl sulfide (DMS) emitted from ocean biota) can introduce H_2SO_4 to the marine atmosphere [*Andreae et al*., 1983].

[29] Aged continental and secondary marine aerosol were characterized by the presence of oxidized organic species in the mass spectra. These oxidized organic aerosols were most likely the photolysis end product of a multitude of more hydrocarbon-like primary emissions [*Jimenez et al*., 2009; *Quinn et al*., 2006; *Q Zhang et al*., 2005b] and were either mixed down from the free troposphere into the MBL or transported in the MBL to the ship location. Both continental and marine aerosol could be mixed down from the upper atmosphere and this aerosol could also be a combination of marine and continental aerosol. For example, aged continental aerosol that was mixed down from the free troposphere to the MBL on 22–23 November 2011 had a lower NH_4^+ to SO_4^{-2} molar ratio than continental aerosol transported in the MBL (0.79 ± 0.03 versus 1.00 ± 0.16). The lower NH_4^+ to SO_4^{-2} molar ratio associated with aerosol from the free troposphere most likely is a result of the nucleation of new particles involving H_2SO_4 from both marine and continental sources and a lack of sources of NH_3 [*Clarke et al*., 1998a; *Clarke et al*., 1998b; *Hegg et al*., 1990; *Zorn et al*., 2008].

[30] Aerosol sampled during a period of high winds and rainfall that accompanies increased convection associated with an MJO event on 24 November showed high concentrations of primary marine aerosol. The measured primary marine aerosol was mainly composed of sea salt as found from IC analysis of filter samples (sea salt is refractory, and thus not effectively measured by the Q-AMS), but some non-refractory submicrometer aerosol was analyzed by the Q-AMS. This aerosol contained *m*/*z* fragments including *m*/*z* 23 (Na^+, from sea salt) and *m*/*z* peaks most likely from $C_2H_5^+$, HCN^+, and $C_3H_3^+$ aerosol fragments which have been associated with primary marine aerosol [*Bates et al*., 2012; *Ovadnevaite et al*., 2011].

[31] These four defined aerosol types were present in varying concentrations throughout the DYNAMO field campaign depending on the dominant aerosol transport direction, meteorological conditions, and oceanic conditions.

4.3. Comparison of Aerosol Properties Observed During DYNAMO to Previous Field Campaigns in the Indian Ocean

[32] HYSPLIT back trajectory calculations for an arrival height of 200 m were used to categorize the impactor sampling periods by the prevailing air mass transport direction (Table 1). Aerosols transported from the north to the ship contained significantly more nss K^+, nss SO_4^{-2}, and NH_4^+ and had higher levels of aerosol light absorption than aerosols transported from other directions (Table 1). During Leg 3, more northerly continental aerosol transport and more submicron aerosol mass were observed than during Leg 2 (Figure 3). Submicrometer nss K^+ and aerosol light absorption were well correlated over all sampling periods ($r^2 = 0.83$), indicating a possible biomass burning source of nss K^+. Submicrometer aerosol light absorption was also correlated, although not as strongly, with submicrometer aerosol mass concentration ($r^2 = 0.75$), NH_4^+ ($r^2 = 0.72$), and SO_4^{-2} ($r^2 = 0.77$). These results suggest that the majority of the submicrometer aerosol mass observed during the experiment, including nss SO_4^{-2}, was transported from the continent and was associated with the K^+ biomass burning component. Additionally, sub-10 micrometer single scattering albedos (SSA) were slightly lower during northerly winds (0.96 ± 0.02) than those measured during southerly winds (0.99 ± 0.01), but these differences are within uncertainties. The close to unity SSA values even for continental aerosol is likely due to the high water uptake from the sulfate and sea salt portion of these particles, which would increase aerosol scattering while aerosol absorption would remain the same. These values were calculated from sub-10 micrometer scattering and absorption coefficients measured at 60% RH and corrected for ambient RH (section 2.4).

[33] The aerosol sources and chemistry observed during DYNAMO were similar to findings from the Indian Ocean Experiment (INDOEX), which took place in the winter and early spring of 1999 in the Indian Ocean [*Quinn et al*., 2002], and the Atmospheric Brown Cloud Post Monsoonal Experiment [*Spencer et al*., 2008], which took place during the shoulder season (boreal fall) of the Asian monsoon in 2004. During INDOEX, the nss SO_4^{2-} and NH_4^+ concentrations in submicrometer aerosol were higher in air masses from the NH versus the SH (0.52 ± 0.18 to 1.8 ± 0.24 and 0.09 ± 0.04 to 0.5 ± 0.12, respectively) (Table 1) [*Quinn et al*., 2002].

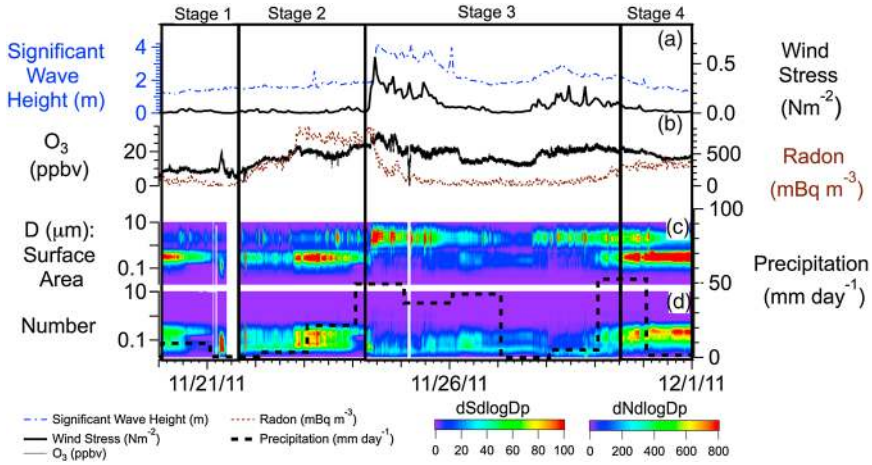

Figure 5. Four stages of aerosol response to MJO-related convection for the November MJO2 event: (a) significant wave height in meters (left axis), wind stress in Nm^{-2} (Figure 5a, right axis), (b) ozone (O_3) concentrations in parts per billion by volume (ppbv) (left axis) and radon in $mBq\,m^{-3}$ (Figure 5b, right axis), (c) surface area concentration of aerosols as a function of aerosol diameter (Figure 5c), (d) number concentration of aerosols as a function of aerosol diameter, and precipitation in $mm\,day^{-1}$ (Figures 5c and 5d, right axis).

In addition, *Quinn et al*. [2002] found that submicrometer aerosols sampled over the NH Indian Ocean had lower single scattering albedos (SSA) at 75% RH (0.91 ± 0.01) than submicrometer aerosols over the SH Indian ocean (1.0 ± 0.02).

[34] *Spencer et al*. [2008] measured the chemical composition of individual aerosol particles 300 nm in diameter and larger to examine the effect of changing circulation patterns associated with the end of the monsoon season on the sources, concentrations, and composition of aerosol transported to the Maldives. They found that northern hemisphere aerosols were enriched in nss SO_4^{-2}, EC, and nss K^+ while SH aerosols were enriched in unreacted sea salt. More NH aerosols were observed later in the fall due to the changing circulation over the Indian Ocean, similar to observations during the latter half of the DYNAMO measurement period.

5. Aerosol Response to the MJO

5.1. Defining Four Stages of Aerosol Response

[35] Two MJO events, one weak (October, MJO1) and one enhanced by a nearby tropical cyclone (November, MJO2), occurred over the Indian Ocean during the DYNAMO aerosol measurement period [*Yoneyama et al*., 2013] (section 3.1). Only the beginning of the weak MJO1 was directly observed onboard the R/V *Revelle* as the ship left station for port shortly after the convectively active MJO cycle began to pass over the central Indian Ocean (Figure 1). The complete MJO2 wave and its effect on aerosol properties, however, were fully observed. Here we present shipboard observations of evolving aerosol properties in the context of the classic MJO convection description to assess the overall effect of the MJO on the regional aerosol and vice versa. Changes in aerosol concentration and properties directly related to MJO convection are discussed in this section. Convection associated with the MJO (rain, wind speed, and wind direction) was found to modify the relative importance of natural and anthropogenic aerosol to the remote marine environment (aerosol types described in section 4.2).

[36] Four stages are defined to describe the aerosol response to the MJO using meteorological and chemical data (significant wave height, wind speed, precipitation, ozone, vertical velocity variance, and radon) and aerosol data (number and surface area size distributions and concentrations) (Figures 5–8). These stages are meant to assist in the description of changes in aerosol concentration and properties during MJO-related convection. More in situ observations or detailed satellite and modeling studies are needed to create statistical definitions of aerosol response to the MJO. Figure 5 shows the meteorological conditions through the full suppressed-active-suppressed MJO2 cycle and the aerosol surface area and number concentration (as a function of aerosol geometric diameter) response to these changing meteorological conditions. Stages 1 and 2 describe the period prior to the passing of the active convective center over the ship location, stage 3 the convectively active phase of the MJO wave, and stage 4 the return to suppressed convection. Only stages 1–3 were clearly observed in Leg 2 (MJO1) while all four stages were fully observed during Leg 3 (MJO2). Here we discuss in detail MJO2 and later compare/contrast MJO1 and MJO2 in terms of their observed effect on the local aerosol population.

[37] Initially, dry conditions associated with the suppressed convection period of the MJO led to a slight build up of sulfate-dominated submicrometer continental aerosol when transport was northerly. Low-wind stress and thus low-wave height also associated with suppressed convection (Figure 5a) resulted in low concentrations of supermicrometer or coarse-mode sea salt aerosol. This dry, calm period is defined as stage 1. During stage 1, the MJO suppressed convection facilitates longer aerosol lifetimes for continental aerosol (low-rain rates) if aerosol transport is from a continental direction while simultaneously reducing the formation of primary marine aerosol (due to low-wind speeds). During stage 2, the local atmosphere became more disturbed with increased vertical mixing and increased precipitation rates. Radon and O_3 increased (Figure 5b) as air masses in the free troposphere were mixed

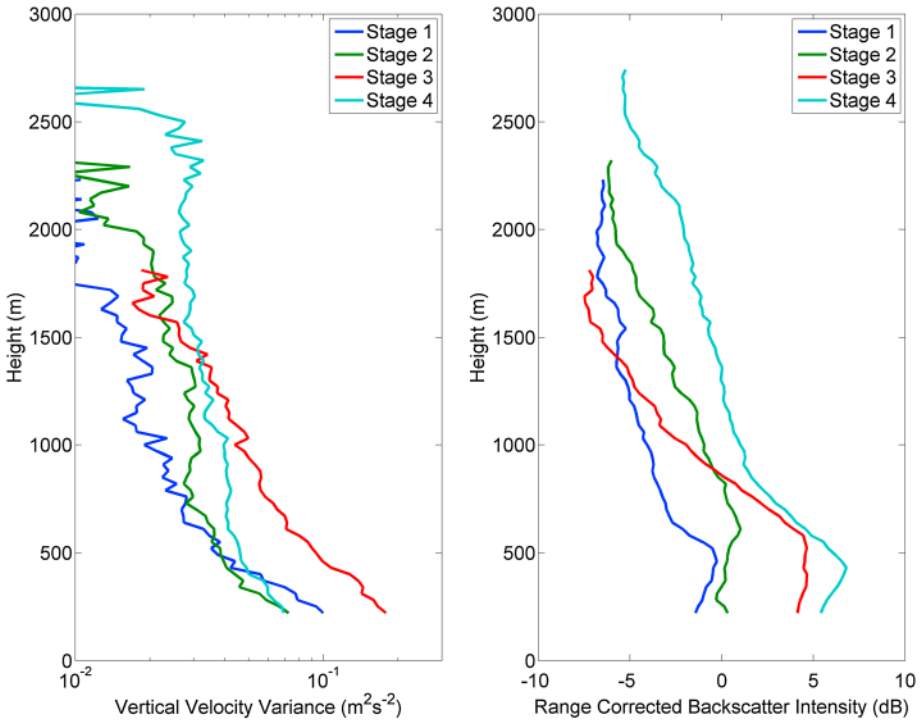

Figure 6. The median Vertical Velocity Variance ($m^2\,s^{-2}$) (Figure 6, left) and (range corrected) aerosol backscatter intensity (dB) (Figure 6, right) profiles calculated as a function of height and aerosol response stage for the MJO2 in November event.

down to the MBL. A few precipitation events occurred during stage 2 (Figure 5c and 5d). Both the aerosol number and surface area concentrations increased with mode diameters at 50 nm and 300 nm, respectively (Figure 5d and 5c). The greatest increase in aerosol number and surface area concentration during stage 2 occurred at 19Z on 22 November 2011, corresponding to a rapid increase in radon indicating that an air mass recently over land was being mixed down into the MBL.

[38] Wind stress and significant wave height increased sharply on 24 November 2011 as the enhanced section of the MJO convective wave moved through, defined here as stage 3 (Figure 5a). Supermicrometer aerosol concentration also rose during this wind burst due to sea salt aerosols being lofted into the atmosphere in response to breaking waves from high winds (Figure 5a) [*O'Dowd and De Leeuw*, 2007]. Figure 6 shows the vertical velocity variance as measured by the HRDL LIDAR (which indicates the

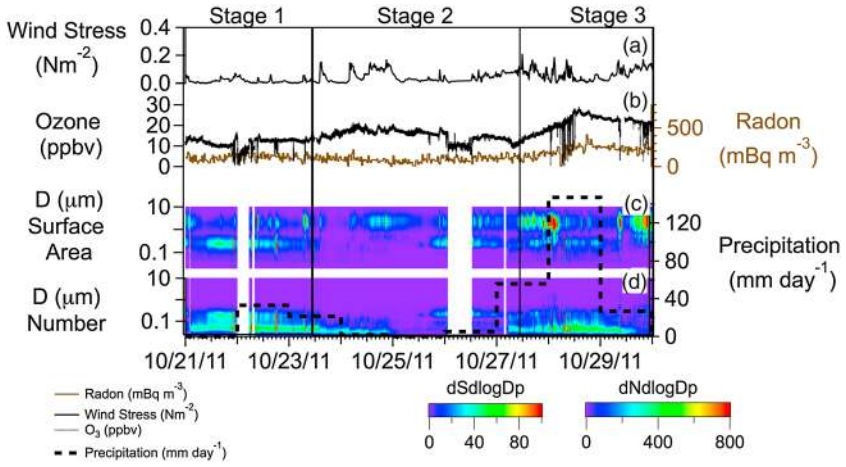

Figure 7. Three observed stages of aerosol response to MJO-related convection for the October MJO1 event: (a) wind stress in Nm^{-2} (left axis), (b) ozone (O_3) concentrations in parts per billion by volume (ppbv) (left axis), and radon in $mBq\,m^{-3}$ (Figure 7b, right axis), (c) surface area concentration of aerosols as a function of aerosol diameter, (d) number concentration of aerosols as a function of aerosol diameter, and accumulated precipitation in $mm\,day^{-1}$ (Figures 7c and 7d, right axis).

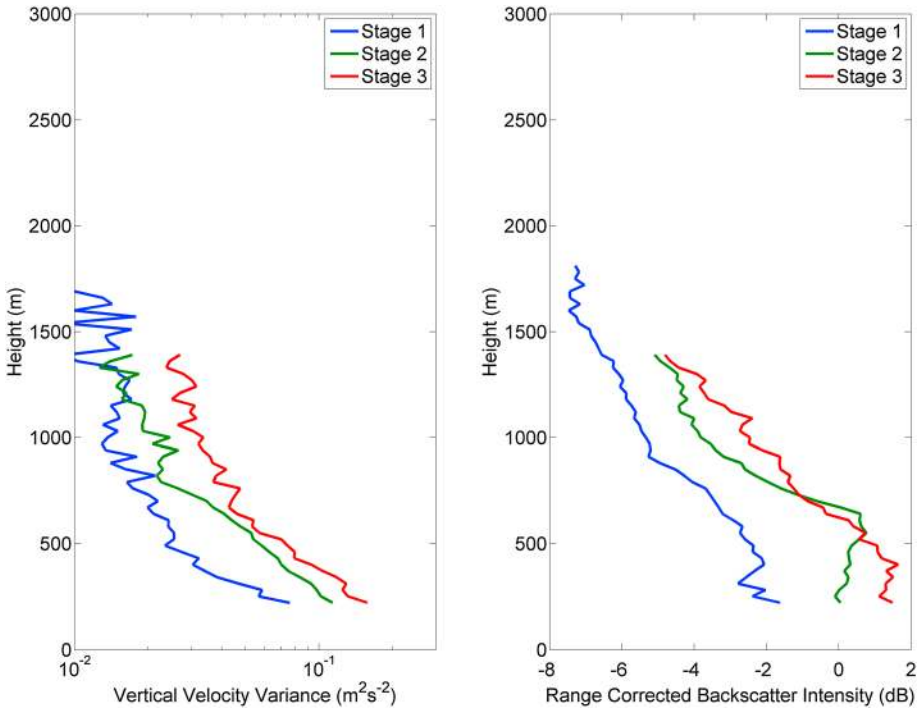

Figure 8. The median Vertical Velocity Variance ($m^2 s^{-2}$) (Figure 8, left) and (range corrected) aerosol backscatter intensity (dB) (Figure 8, right) profiles calculated as a function of height and aerosol response stage for the MJO1 event in October. There is no stage 4 profile as the ship left the observational area prior to the onset of that stage.

strength of vertical motion in the atmosphere) and aerosol backscatter intensity (range corrected) as a function of altitude, averaged over the defined MJO aerosol response stages. Progressing from stage 1 to stage 3, there is an increase in mixing and vertical transport (as indicated by the vertical velocity variance) and an associated increase in the concentration of sea salt aerosol, extended through the MBL, to a height of 1000 m (as indicated by the increase in aerosol backscatter intensity in Figure 6). At the beginning of stage 3 and again on 28 November 2011, there is a sharp increase in the strength of the vertical velocity variance and aerosol backscatter to a height of 1000 m (Figures 1 and 6). Bursts of increased, deep vertical velocity variance were observed late in stage 2, and these bursts transitioned into a sustained increase in vertical velocity variance through atmospheric heights of 1000 m or greater during stage 3 (Figures 1 and 6). The average vertical velocity variance and transport during the MJO-related convection was more sustained and, averaged over the time of the convectively active wave (stage 3), greater than during convectively suppressed periods at lower altitudes for both MJO1 and MJO2 (Figures 8 and 6, respectively). Backscatter intensity (from supermicrometer—i.e., sea salt—aerosols) is also shown to increase in stage 3 as sea salt aerosol is lofted into the atmosphere. This effect persists through stage 4 as some of the sea salt aerosol remained in the atmosphere after the winds reduced in speed.

[39] As the MJO2 progressed, heavy precipitation led to the wet deposition of submicrometer aerosol, and the atmosphere was left clean aside from sea salt during periods of high winds and some continuous mixing down of small particles from the upper troposphere (stage 3). During stage 3, the air mass transport direction, as calculated by HYSPLIT back trajectories, was primarily south-easterly (background marine). Stage 4 shows a return to suppressed convection based on measured reduced wave height and wind stress. Northerly flow during late November/early December (from HYSPLIT backtrajectory calculations) quickly reintroduced submicrometer continental aerosol to the local MBL as the precipitation decreased.

5.2. Comparison of MJO1 and MJO2

[40] Figure 7 shows the meteorological data (wind stress, O_3, radon, precipitation) and aerosol concentration as a function of geometric diameter for aerosol surface area and aerosol number for stages 1, 2, and 3 of the weak MJO event observed in the eastern Indian Ocean in October (Yoneyama et al., submitted manuscript, 2013). Like stage 1 for MJO2, stage 1 for MJO1 is characterized by low levels of wind stress and thus low levels of primary marine (sea salt) supermicrometer aerosols. Some buildup of submicrometer aerosols can be observed; however, as the primary aerosol transport direction during the month of October was southerly (clean marine) rather than northerly (continental), aerosol levels were generally low. During stage 2, periods of higher wind stress began to occur (increasing supermicrometer aerosol) and O_3 began to rise (as submicrometer aerosol was transported from the upper atmosphere into the MBL). Radon remained low for the entire MJO1 period, indicating that there was little continental influence on the aerosol population during this MJO cycle. During MJO1, there was no sharply defined wind burst initiating the convectively active stage; rather, for MJO1, stage 3 is defined by a burst of enhanced rainfall accompanied by an increase in O_3 and small increases

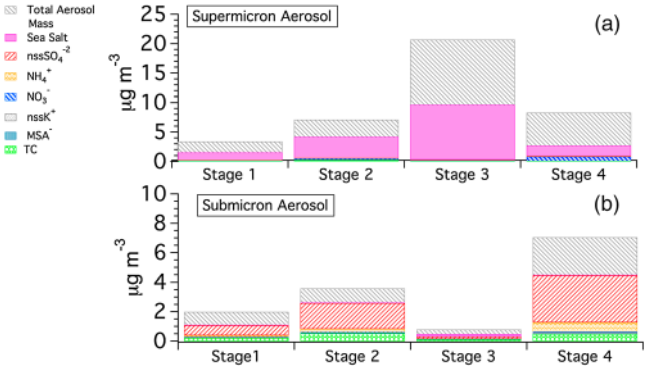

Figure 9. The aerosol sub- and supermicrometer chemistry for the stages of aerosol response to the MJO convection. (a) Supermicrometer aerosol chemistry and (b) submicrometer aerosol chemistry. Total aerosol mass is gravimetric mass measured at 60% RH. The disparity between total aerosol mass and measured chemical mass is due to water at 60% RH and unanalyzed chemical mass (e.g., dust).

in wind stress. Figure 8 shows the vertical velocity variance and range corrected backscatter intensity for MJO1 stages 1–3. Again, stage 3 shows the highest vertical velocity variance and an increase in the aerosol backscatter through 1500 m in altitude from the less convectively active stages.

[41] An aerosol size regime change from submicrometer to supermicrometer was observed in the MJO1 similar to that observed in the MJO2 (section 5.1); however, the low initial aerosol levels (due to the more southerly aerosol transport direction) and the lower wind stress levels in stage 3 of MJO1 versus MJO2 reduced the net effect on MJO-related convection on aerosol. Likely, the defined aerosol responses to MJO convection occur for each MJO convection cycle that occurs over the Indian Ocean but the magnitude of the effect on the remote marine aerosol population varies with the seasons.

5.3. MJO-Related Convection and Aerosol Chemical Composition

[42] While the MJO may increase the lifetime of continental aerosol transported to the Indian Ocean, and changes in circulation due to the MJO may introduce new continental aerosol to the MBL, the MJO's most dramatic effect on aerosol chemistry is the rainout of primarily sulfate submicrometer aerosol particles (both marine and continental in origin) and the introduction of fresh supermicrometer sea salt particles to the MBL. The total mass concentration of supermicrometer and submicrometer aerosol changed significantly as the MJO convection progressed from suppressed (stage 1) to increasingly active (stages 2–3) and back to suppressed (stage 4) (Figure 9). Shown in Figure 9 is the chemical speciation of sub- and supermicrometer aerosol from filter-based impactor IC and gravimetric data. Impactor measurements were used here instead of the Q-AMS real-time data because the Q-AMS is unable to quantitatively measure submicrometer refractory species (such as sea salt) and cannot measure any supermicrometer particles. Note that the total gravimetric mass shown of the bulk sub- and supermicrometer aerosol includes both dust and water (at 60% RH) and thus is greater than the sum of the chemically analyzed mass. Additionally, some mass from organic aerosol may be part of the unknown mass as $\mu g\,C\,m^{-3}$ not total particulate organic mass was measured.

[43] Due to high winds and heavy precipitation during stage 3, the submicrometer aerosol concentration was drastically reduced and supermicrometer sea salt aerosol (NaCl) dominated the aerosol mass. Sea salt was the primary component of the submicrometer as well as supermicrometer aerosol mass during stage 3. Conversely, during stages 1, 2, and 4, the concentration of submicrometer aerosol increased relative to sea salt due to northerly transport of continental air and lower wind speeds reducing the emission of primary marine aerosol from the ocean surface. Wind direction and aerosol transport would change the characteristics of aerosol during these stages (i.e., southerly background marine in the boreal fall and spring, northerly in the boreal late fall and winter). Continental influence was greatest in stage 4 as even the supermicrometer aerosol was affected by anthropogenic influence. NO_3^- (from HNO_3 uptake by sea salt) increased in concentration in comparison to the fresher, primarily marine-influenced supermicrometer aerosol that was sampled during stage 3.

5.4. The Effect of the MJO on Aerosol Number and Cloud Condensation Nuclei (CCN) Concentrations

[44] As the aerosol chemistry and aerosol mass changed, the aerosol number concentration and size distribution also changed during the MJO progression for both the MJO1 (Figure 10a, stages 1–3) and the MJO2 event (Figure 10b, stages 1–4). Aerosol number concentration, rather than surface area or volume, controls cloud condensation nuclei (CCN) concentrations. During MJO2, the aerosol number concentration was higher during the suppressed periods (stages 1, 2, and 4) due to the dry conditions and northerly flow associated with the end of the Asian monsoon season. The number size distribution was bimodal with an Aitkin mode peak around 50 nm from particles mixed into the MBL from the free troposphere and an accumulation mode at approximately 200–300 nm (at 60% ± 10% RH) resulting from cloud processing of the Aitken mode particles. These largely sulfate submicrometer aerosol particles

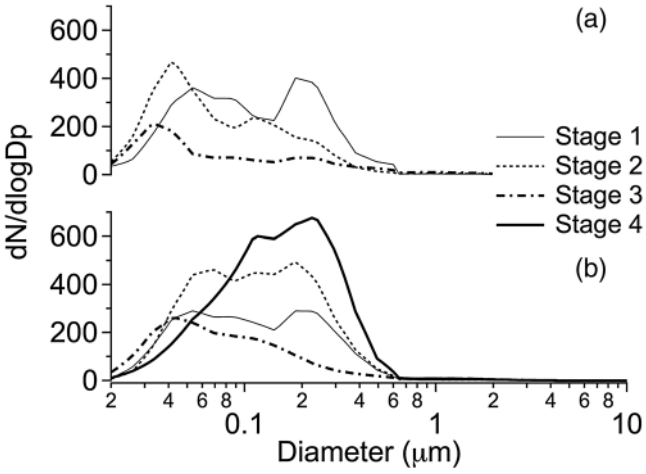

Figure 10. (a) Aerosol number size distribution at 60% relative humidity during stages 1–3 of the MJO-related convection in October and (b) during all four stages of the MJO-related convection in November.

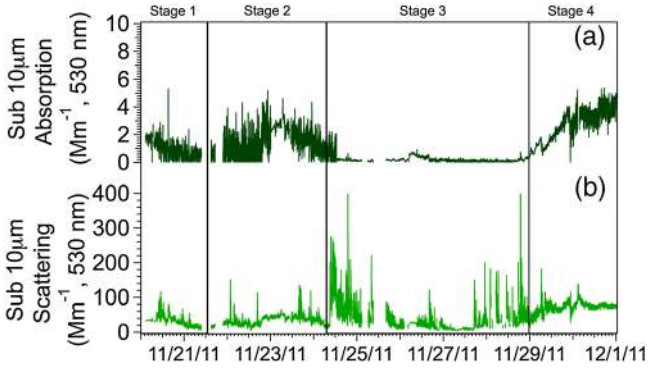

Figure 11. (a) The sub-10 micrometer aerosol absorption and (b) scattering at 530 nm.

(e.g., Figure 9) could nucleate water and act as CCN for supersaturations typical of MBL clouds in the region [*Kohler*, 1936]. Based on an ammonium bisulfate composition, 200 to 300 nm particles (accumulation mode) activate at a critical supersaturation of 0.1% or less while the smaller 50 nm particles (Aitken mode) would need a higher supersaturation (>0.5%) to activate [*Petters and Kreidenweis*, 2007]. Supersaturations at tropical maritime cloud bases typically do not exceed 0.5% [*Khain et al*., 2012]. However, supersaturations within tropical clouds are on average 0.5–2% and can be upwards of 20% during periods of deep convection. Thus, smaller particles may be important in CCN [*Khain et al*., 2012]. The interplay between aerosol and clouds is complex such that more CCN does not necessarily equate to more cloud cover. The hydrological cycle, radiative balance, and wider-scale weather patterns have greater effects on cloudiness and precipitation than aerosols and thus may reduce the effects aerosols have on local convection [*Stevens and Feingold*, 2009]. The MJO is governed by large-scale convection and ocean conditions and thus any aerosol effect may be small to negligible, though some aerosol effect on local weather patterns may still be important.

[45] *Rosenfeld et al*. [2008] suggest that there is an aerosol level in the tropics that results in optimal cloud development over both the land and the ocean. Using a simple model, *Rosenfeld et al*. [2008] found that a CCN concentration of 1200 cm^{-3} at 0.4% supersaturation, corresponding to an aerosol optical thickness of 0.25, causes maximum convective available potential energy to be consumed by clouds and storm systems in the area. Increases in CCN concentration can lead to a decrease in the CCN coalescence rate and thus a delay of rainfall [*Twomey and Warner*, 1967]. Delaying the conversion of CCN to rain droplets allows clouds to ascend higher in the atmosphere past the freezing level. Past a CCN concentration of approximately 1200 cm^{-3} and an AOT of 0.25, the reduction in solar radiation reaching the surface due to the aerosol layer lowers the surface heating and thus could in theory reduce convection [*Bell et al*., 2008; *Rosenfeld et al*., 2008], At the DYNAMO field site, submicrometer aerosol number concentrations were on average <300 cm^{-3}, more typical of remote marine than polluted conditions [*Pruppacher and Klett*, 1997; *Roberts et al*., 2006]. The total number of aerosol particles available as CCN before the MJO event increased from 250 cm^{-3} during October to 570 cm^{-3} during November. The aerosol concentration limit where aerosol begins to suppress convection was not reached in these measurements [*Rosenfeld et al*., 2008].

[46] During the MJO rainfall event, background and continental aerosols were removed by wet deposition and primary marine aerosol increased due to the higher wind speeds. Like the submicrometer sulfate aerosols, the coarse-mode sea salt aerosols can act as CCN, although their number concentration was much less. The incorporation of a few of these larger sized sea salt aerosols into clouds has been shown in some cases to increase rainout rates as opposed to an increase in more numerous but smaller submicrometer CCN, though giant (5–10 μm) CCN were found to have the greatest effect [*Rudich et al*., 2002].

5.5. MJO and Aerosol: Comparison to Previous Observations

[47] Although this work only measures aerosol in the lower atmosphere (18 m for most measurements and up to 1500 m for supermicrometer aerosol backscatter intensity), not total AOT, we found a similar relationship between the removal of absorbing aerosol and rainfall associated with the MJO as that found by *Tian et al*. [2008]. The SSA increased to near unity during the convective stage of the MJO as the sub-10 micrometer absorption decreased sharply (Figure 11a) and the scattering from sea salt aerosols increased during the highest wind periods (Figure 11b). Again, note that these measurements are made at 18 m over the ocean surface and may not be representative of the AOT, which was measured by the studies cited in this section. In remote background marine regions with low-wind speeds, enhanced convection from the MJO would increase sea salt aerosol in the local atmosphere relative to conditions typical of the equatorial ocean. Therefore, the MJO convection could enhance AOT. This increase in AOT may explain the weakly positive correlation [*Tian et al*., 2008] between MJO rainfall and AOT. Additionally, previous work has found a possible relationship between increased ocean productivity and MJO-related convection which could also contribute to the enhancement of AOT during the active MJO phase [*Tian and Waliser*, 2012; *Waliser et al*., 2005] as increased wind has been shown to correlate with increased biological productivity on the ocean surface [*Chapman et al*., 2002]. We do not observe an increase in MSA^- during stage 3, but we do observe a slight increase during stage 4 (Figure 3 from 28 November onwards). MSA^- is formed from the photolysis of DMS emitted by ocean biota. There may be a small convection-driven effect on secondary marine aerosol production (only one data point is available) but this effect appears to be delayed until the second suppressed convection phase as MSA^- is formed and builds up in the atmosphere. Enhancement of supermicrometer sea salt aerosol is the greatest observed effect of the MJO on aerosol. The reduction in the already low submicrometer aerosol due to rainout in a calm remote marine location would potentially not have as great of an effect on AOT as the wind-driven enhancement of sea salt aerosol.

5.6. Putting the Pieces Together

[48] The seasonal reversal of wind direction over the Indian Ocean accompanying the beginning of the boreal winter dry season in Asia, as well as two MJO events, were observed during the DYNAMO 2011 field campaign. Aerosols from both marine and continental sources were measured over the remote equatorial Indian Ocean during

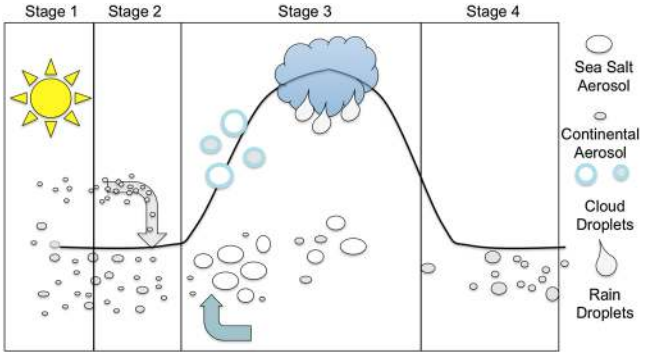

Figure 12. A representative cartoon of the aerosol response to MJO-related convection. Stage 1: Suppressed convection, longer aerosol lifetime. Stage 2: Disturbed convection, overturning of the troposphere, and introduction of aerosol from the upper atmosphere. Stage 3: Enhanced wind and precipitation, increased sea salt aerosol mass, eventual rainout of aerosol. Stage 4: Return to suppressed convection.

the boreal fall of 2011 onboard the R/V *Revelle* as part of the DYNAMO 2011 field campaign. During this measurement period, the winds transitioned from predominately southerly (Asian monsoon season) to predominately northerly (Asian dry season). With this reversal of wind direction came a shift in aerosol properties, from primarily background marine aerosol observed in October to more continentally influenced aerosol in November and early December. The more continentally influenced air mass had higher submicrometer aerosol concentrations and increased aerosol light absorption. Drier conditions and northerly air flow during boreal winter have previously been associated with increased continental aerosol over the remote Indian Ocean [*Ramanathan et al*., 2001].

[49] During October and November 2011, the aerosol response to a partial (October) and a full (November) cycle of an MJO wave was observed on the equatorial Indian Ocean. From these data, four stages in the aerosol response to the MJO wave were identified and are summarized in cartoon form in Figure 12.

[50] 1. Low rainout rates associated with the convectively suppressed period of the MJO increase the lifetime of submicrometer aerosol in the marine atmosphere allowing concentrations of submicrometer aerosol to build up.

[51] 2. Tropospheric turnover just prior to the MJO event introduces aerosol from the upper atmosphere. These particles, primarily $SO4^{-2}$, are of a size to act as CCN at supersaturations of 0.1% (for the 200–300 nm number mode diameter aerosol) and 0.5% or greater (for the 50 nm number mode diameter aerosol).

[52] 3. High surface wind speeds increase the concentration of sub- and supermicrometer primary ocean-derived particles (sea spray), both of which could also act as CCN. Rains quickly following the initial wind burst remove submicrometer aerosol through wet deposition, while high wind bursts continuously resupply sea spray aerosol.

[53] 4. As the convectively active period ends and the wind speeds return to suppressed levels, primary sea spray aerosol decreases and submicrometer secondary aerosol from the free troposphere builds up again in the MBL.

6. Conclusions

[54] From the measurements presented in this work, we have determined that MJO-associated convection does not solely affect aerosol by rainout; rather, increased wind speeds during convectively active periods greatly enhances the concentration of sea salt aerosols over the equatorial Indian Ocean and downward motion in the atmosphere just prior to and during the MJO enhanced convection introduces new submicrometer particles to the MBL. Suppressed convection periods could lead to longer aerosol lifetimes and thus longer aerosol transport distances, although the interplay between the beginning of the Asian winter dry season and the MJO events observed makes the exact magnitude of this effect difficult to determine.

[55] Likely, the four defined stages in aerosol response to MJO convection (section 5) occur during each MJO event; however, the net effect would vary with each MJO wave, with interference from coinciding meteorology, and with the ambient aerosol population. Increased continental transport during the beginning of the Asian dry season would enhance the effect of stages 1, 2, and 4. An increase in CCN concentrations during the suppressed phase from longer aerosol lifetime and transport could lead to more energetic convection [*Bell et al*., 2008; *Rosenfeld et al*., 2008]. In general, the MJO signal peaks in boreal winter and spring [*Zhang*, 2005], which coincides with the Asian dry season, the formation of the Indo-Asian Haze layer in Asia [*Ramanathan et al*., 2001], and increased northerly flow over the Indian Ocean. Stronger MJO-related convection thus overlaps with higher aerosol concentrations, and the effect of the MJO on the aerosol population could be greatly enhanced in the boreal winter. While a multitude of meteorological and oceanographic factors affect the initiation and propagation of the MJO, it is possible submicrometer continental aerosol from Asia could have some influence in enhancing MJO-associated convection as the MJO itself changes the aerosol population and concentration. Modeling work is needed to fully explore the effect of aerosols, and specifically continental and anthropogenic aerosols, on the MJO. Regardless of anthropogenic influence, MJO-related convection has been shown to have a large effect on the aerosol population over the equatorial ocean.

[56] **Acknowledgments.** The authors would like to acknowledge the National Research Council and the NOAA Climate Program Office (CPO Earth System Science Program) for funding H. Langley DeWitt and the aerosol measurement component of the DYNAMO research project. We would also like to acknowledge the captain and crew of the R/V *Revelle* as well as Chief Scientist Jim Moum and the other scientists onboard the *Revelle* for their help facilitating this science cruise and the scientific discussions onboard. Alexander Smirnov at NASA Aeronet analyzed the Microtops AOT data. Ludovich Bariteau at NOAA ESRL provided the wind stress and significant wave height data reported in the paper. Thanks also go to James Johnson and Drew Hamilton at the Joint Institute for the Study of the Atmosphere and Ocean (JISAO) for their help with instrument calibration and shipping.

References

Anderson, T. L., and J. A. Ogren (1998), Determining aerosol radiative properties using the TSI 3563 integrating nephelometer, *Aerosol Sci. Tech.*, *29*(1), 57–69.

Andreae, M. O., W. R. Barnard, and J. M. Ammons (1983), The biological production of dimethylsulfide in the ocean and its role in the global atmospheric sulfur budget, *Ecol. Bull.*, *35*, 167–177.

Annamalai, H., and J. M. Slingo (2001), Active/break cycles: Diagnosis of the intraseasonal variability of the Asian Summer Monsoon, *Clim. Dynam.*, *18*(1-2), 85–102.

Bates, T. S., D. J. Coffman, D. S. Covert, and P. K. Quinn (2002), Regional marine boundary layer aerosol size distributions in the Indian, Atlantic, and Pacific Oceans: A comparison of INDOEX measurements with

ACE-1, ACE-2, and Aerosols99, *J. Geophys. Res. Atmos.*, *107*(D19), 8026, doi:10.1029/2001JD001174.

Bates, T. S., P. K. Quinn, D. J. Coffman, J. E. Johnson, and A. M. Middlebrook (2005), Dominance of organic aerosols in the marine boundary layer over the Gulf of Maine during NEAQS 2002 and their role in aerosol light scattering, *J. Geophys. Res. Atmos.*, *110*, D18202, doi:10.1029/2005JD005797.

Bates, T. S., et al. (2008), Boundary layer aerosol chemistry during TexAQS/GoMACCS 2006: Insights into aerosol sources and transformation processes, *J. Geophys. Res. Atmos.*, *113*, D00F01, doi:10.1029/2008JD010023.

Bates, T. S., et al. (2012), Measurements of ocean derived aerosol off the coast of California, *J. Geophys. Res. Atmos.*, *117*, D00V15, doi:10.1029/2012JD017588.

Bell, T. L., D. Rosenfeld, K. M. Kim, J. M. Yoo, M. I. Lee, and M. Hahnenberger (2008), Midweek increase in US summer rain and storm heights suggests air pollution invigorates rainstorms, *J. Geophys. Res. Atmos.*, *113*, D02209, doi:10.1029/2007JD008623.

Berner, A., C. Lurzer, F. Pohl, O. Preining, and P. Wagner (1979), Size distribution of the urban aerosol in Vienna, *Sci. Total Environ.*, *13*(3), 245–261.

Canagaratna, M. R., et al. (2007), Chemical and microphysical characterization of ambient aerosols with the aerodyne aerosol mass spectrometer, *Mass Spectrom. Rev.*, *26*(2), 185–222.

Chapman, E. G., W. J. Shaw, R. C. Easter, X. Bian, and S. J. Ghan (2002), Influence of wind speed averaging on estimates of dimethylsulfide emission fluxes, *J. Geophys. Res. Atmos.*, *107*(D23), 4672, doi:10.1029/2001JD001564.

Clarke, A. D., J. L. Varner, F. Eisele, R. L. Mauldin, D. Tanner, and M. Litchy (1998a), Particle production in the remote marine atmosphere: Cloud outflow and subsidence during ACE 1, *J. Geophys. Res. Atmos.*, *103*(D13), 16397–16409.

Clarke, A. D., et al. (1998b), Particle nucleation in the tropical boundary layer and its coupling to marine sulfur sources, *Science*, *282*(5386), 89–92.

Dasgupta, S., R. P. Singh, and M. Kafatos (2009), Comparison of global chlorophyll concentrations using MODIS data, *Adv. Space Res.*, *43*(7), 1090–1100.

DeCarlo, P. F., et al. (2006), Field-deployable, high-resolution, time-of-flight aerosol mass spectrometer, *Anal Chem*, *78*(24), 8281–8289.

Grund, C. J., R. M. Banta, J. L. George, J. N. Howell, M. J. Post, R. A. Richter, and A. M. Weickmann (2001), High-resolution Doppler lidar for boundary layer and cloud research, *J. Atmos. Ocean. Tech.*, *18*(3), 376–393.

Hegg, D. A., L. F. Radke, and P. V. Hobbs (1990), Particle-production associated with marine clouds, *J. Geophys. Res. Atmos.*, *95*(D9), 13917–13926.

Jimenez, J. L., et al. (2009), Evolution of organic aerosols in the atmosphere, *Science*, *326*(5959), 1525–1529.

Kessler, W. S., and M. J. McPhaden (1995), Oceanic equatorial waves and the 1991–93 El-Nino, *J. Climate*, *8*(7), 1757–1774.

Khain, A. P. P., V. Phillips, N. Benmoshe, A. Pokrovsky (2012), The role of small soluble aerosols in the microphysics of deep maritime clouds, *J. Atmos. Sci.*, *69*, 20.

Kohler, H. (1936), The nucleus in and the growth of hygroscopic droplets, *T. Faraday Soc.*, *43*, 9.

Lau, A. K. H., and D. Waliser (2012), *Intraseasonal Variability in the Atmosphere-Ocean Climate System*, p. 613, Springer-Praxis Books in Environmental Sciences, Heidelberg, Germany.

de Leeuw, G., E. L. Andreas, M. D. Anguelova, C. W. Fairall, E. R. Lewis, C. O'Dowd, M. Schulz, and S. E. Schwartz (2011), Production flux of sea spray aerosol, *Rev. Geophys.*, *49*, RG2001, doi:10.1029/2010RG000349.

Li, K.-F., B. Tian, D. E. Waliser, and Y. L. Yung (2010), Tropical mid-tropospheric CO2 variability driven by the Madden–Julian oscillation, *Proceedings of the National Academy of Sciences*.

Liebmann, B., G. N. Kiladis, C. S. Vera, A. C. Saulo, and L. M. V. Carvalho (2004), Subseasonal variations of rainfall in South America in the vicinity of the low-level jet east of the Andes and comparison to those in the South Atlantic convergence zone, *J. Climate*, *17*(19), 3829–3842.

Madden, R. A., and P. R. Julian (1972), Description of global-scale circulation cells in the tropics with a 40-50 Day Period, *J. Atmos. Sci.*, *29*, 15.

O'Dowd, C. D., and G. De Leeuw (2007), Marine aerosol production: A review of the current knowledge, *Philos. T. R. Soc. A*, *365*(1856), 1753–1774.

O'Dowd, C. D., B. Langmann, S. Varghese, C. Scannell, D. Ceburnis, and M. C. Facchini (2008), A combined organic-inorganic sea-spray source function, *Geophys. Res. Lett.*, *35*, L01801, doi:10.1029/2007GL030331.

Ovadnevaite, J., C. O'Dowd, M. Dall'Osto, D. Ceburnis, D. R. Worsnop, and H. Berresheim (2011), Detecting high contributions of primary organic matter to marine aerosol: A case study, *Geophys. Res. Lett.*, *38*, L02807, doi:10.1029/2010GL046083.

Petters, M. D., and S. M. Kreidenweis (2007), A single parameter representation of hygroscopic growth and cloud condensation nucleus activity, *Atmos. Chem. Phys.*, *7*(8), 1961–1971.

Pruppacher, H. R., and J. D. Klett (1997), *Microphysics of Clouds and Precipitation*, 2nd rev. and enl. ed., xx, 954 pp., Kluwer Academic Publishers, Dordrecht; Boston.

Quinn, P. K., and T. S. Bates (2011), The case against climate regulation via oceanic phytoplankton sulphur emissions, *Nature*, *480*(7375), 51–56.

Quinn, P. K., and D. J. Coffman (1998), Local closure during the first aerosol characterization experiment (ACE 1): Aerosol mass concentration and scattering and backscattering coefficients, *J. Geophys. Res. Atmos.*, *103*(D13), 16575–16596.

Quinn, P. K., D. J. Coffman, T. S. Bates, T. L. Miller, J. E. Johnson, E. J. Welton, C. Neususs, M. Miller, and P. J. Sheridan (2002), Aerosol optical properties during INDOEX 1999: Means, variability, and controlling factors, *J. Geophys. Res. Atmos.*, *107*(D19), 8020, doi:10.1029/2000JD000037.

Quinn, P. K., et al. (2006), Impacts of sources and aging on submicrometer aerosol properties in the marine boundary layer across the Gulf of Maine, *J. Geophys. Res. Atmos.*, *111*, D23S36, doi:10.1029/2006JD007582.

Quinn, P. K., T. S. Bates, D. J. Coffman, and D. S. Covert (2008), Influence of particle size and chemistry on the cloud nucleating properties of aerosols, *Atmos. Chem. Phys.*, *8*(4), 1029–1042.

Ramanathan, V., et al. (2001), Indian Ocean experiment: An integrated analysis of the climate forcing and effects of the great Indo-Asian haze, *J. Geophys. Res. Atmos.*, *106*(D22), 28371–28398.

Reid, J. S., P. Xian, E. J. Hyer, M. K. Flatau, E. M. Ramirez, F. J. Turk, C. R. Sampson, C. Zhang, E. M. Fukada, and E. D. Maloney (2012), Multi-scale meteorological conceptual analysis of observed active fire hotspot activity and smoke optical depth in the Maritime Continent, *Atmos. Chem. Phys.*, *12*(4), 2117–2147.

Roberts, G., G. Mauger, O. Hadley, and V. Ramanathan (2006), North American and Asian aerosols over the eastern Pacific Ocean and their role in regulating cloud condensation nuclei, *J. Geophys. Res. Atmos.*, *111*, D13205, doi:10.1029/2005JD006661.

Rosenfeld, D., U. Lohmann, G. B. Raga, C. D. O'Dowd, M. Kulmala, S. Fuzzi, A. Reissell, and M. O. Andreae (2008), Flood or drought: How do aerosols affect precipitation?, *Science*, *321*(5894), 1309–1313.

Rudich, Y., O. Khersonsky, and D. Rosenfeld (2002), Treating clouds with a grain of salt, *Geophys. Res. Lett.*, *29*(22), 2060, doi:10.1029/2002GL016055.

Smirnov, A., et al. (2009), Maritime aerosol network as a component of aerosol robotic network, *J. Geophys. Res. Atmos.*, *114*, D06204, doi:10.1029/2008JD011257.

Spencer, M. T., J. C. Holecek, C. E. Corrigan, V. Ramanathan, and K. A. Prather (2008), Size-resolved chemical composition of aerosol particles during a monsoonal transition period over the Indian Ocean, *J. Geophys. Res. Atmos.*, *113*, D16305, doi:10.1029/2007JD008657.

Stevens, B., and G. Feingold (2009), Untangling aerosol effects on clouds and precipitation in a buffered system, *Nature*, *461*(7264), 607–613.

Tian, B. J., and D. Waliser (2012), Madden-Julian Oscillation, in *Encyclopedia of Remote Sensing*, edited by E. Njoku, pp. 569-584, SpringerReference, Berlin Heidelberg.

Tian, B. J., Y. L. Yung, D. E. Waliser, T. Tyranowski, L. Kuai, E. J. Fetzer, and F. W. Irion (2007), Intraseasonal variations of the tropical total ozone and their connection to the Madden-Julian Oscillation, *Geophys. Res. Lett.*, *34*, L08704, doi:10.1029/2007GL029451.

Tian, B. J., D. E. Waliser, R. A. Kahn, Q. Li, Y. L. Yung, T. Tyranowski, I. V. Geogdzhayev, M. I. Mishchenko, O. Torres, and A. Smirnov (2008), Does the Madden-Julian oscillation influence aerosol variability?, *J. Geophys. Res. Atmos.*, *113*, D12215, doi:10.1029/2007JD009372.

Tucker, S. C., W. A. Brewer, R. M. Banta, C. J. Senff, S. P. Sandberg, D. C. Law, A. M. Weickmann, and R. M. Hardesty (2009), Doppler lidar estimation of mixing height using turbulence, shear, and aerosol profiles, *J. Atmos. Ocean Tech.*, *26*(4), 673–688.

Twomey, S., and J. Warner (1967), Comparison of measurements of cloud droplets and cloud nuclei, *J. Atmos. Sci.*, *24(6)*, 702–703.

Waliser, D. E., R. Murtugudde, P. Strutton, and J. L. Li (2005), Subseasonal organization of ocean chlorophyll: Prospects for prediction based on the Madden-Julian Oscillation, *Geophys. Res. Lett.*, *32*, L23602, doi:10.1029/2005GL024300.

Wheeler, M. C., and H. H. Hendon (2004), An all-season real-time multivariate MJO index: Development of an index for monitoring and prediction, *Mon. Weather Rev.*, *132*(8), 1917–1932.

Whittlestone, S., and W. Zahorowski (1998), Baseline radon detectors for shipboard use: Development and deployment in the first aerosol characterization experiment (ACE 1), *J. Geophys. Res. Atmos.*, *103*(D13), 16743–16751.

Yoneyama, K., C. Zhang, and C. N. Long (2013), Tracking pulses of the Madden-Julian Oscillation, *B Am Meteorol Soc.*, doi:10.1175/BAMS-D-12-00157.1.

Zhang, C. (2005), Madden-Julian oscillation, *Rev. Geophys.*, *43*, RG2003, doi:10.1029/2004RG000158.

Zhang, Q., M. R. Canagaratna, J. T. Jayne, D. R. Worsnop, and J. L. Jimenez (2005a), Time- and size-resolved chemical composition of submicron particles in Pittsburgh: Implications for aerosol sources and processes, *J. Geophys. Res. Atmos.*, *110*, D07S09, doi:10.1029/2004JD004649.

Zhang, Q., M. R. Alfarra, D. R. Worsnop, J. D. Allan, H. Coe, M. R. Canagaratna, and J. L. Jimenez (2005b), Deconvolution and quantification of hydrocarbon-like and oxygenated organic aerosols based on aerosol mass spectrometry, *Environ. Sci. Technol.*, *39*(13), 4938–4952.

Zorn, S. R., F. Drewnick, M. Schott, T. Hoffmann, and S. Borrmann (2008), Characterization of the South Atlantic marine boundary layer aerosol using an aerodyne aerosol mass spectrometer, *Atmos. Chem. Phys.*, *8*(16), 4711–4728.